Journal of Fluorine Chemistry 129 (2008) 621–624

Contents lists available at ScienceDirect

Journal of Fluorine Chemistry

journal homepage: www.elsevier.com/locate/fluor

Synthesis and spectral properties of Eu^{3+}-doped YF_3 nanobundles

Guofeng Wang [a], Weiping Qin [a,*], Jisen Zhang [b], Jishuang Zhang [b], Yan Wang [b], Chunyan Cao [b], Lili Wang [a], Guodong Wei [a], Peifen Zhu [a], Ryongjin Kim [a]

[a] State Key Laboratory on Integrated Optoelectronics, College of Electronic Science & Engineering, Jilin University, Changchun 130012, PR China
[b] Key Laboratory of Excited State Processes, Changchun Institute of Optics, Fine Mechanics and Physics, Chinese Academy of Science, Changchun 130033, PR China

ARTICLE INFO

Article history:
Received 1 February 2008
Received in revised form 4 May 2008
Accepted 5 May 2008
Available online 13 May 2008

Keywords:
Microemulsion
Nanowhiskers
Luminescence
Concentration quenching

ABSTRACT

YF_3:Eu^{3+} nanobundles were synthesized by a facile microemulsion method. Analysis of X-ray diffraction, scanning electron microscope, and transmission electron microscopy reveals that each nanobundle consists of numerous nanowhiskers with a mean length of ~500 nm and a mean diameter of ~2 nm. Under 393-nm excitation, the luminescence was dominated by $^5D_0 \rightarrow {}^7F_1$ transition, indicating the inversion symmetry of Eu^{3+} site. The luminescence intensity increased with increasing Eu^{3+} concentration, up to about 30 mol%, and then decreased abruptly. The peak positions and spectral shapes of emissions were independent of Eu^{3+} concentration. Finally, the critical distance of energy transfer was calculated.

1. Introduction

Doped nanomaterials have attracted increasing attention since 1994 [1], when Bhargava et al. reported that doped nanocrystalline phosphors yielded high luminescence efficiencies. With rapidly shrinking size, nanomaterials usually exhibit novel physical and chemical properties, and therefore are novel functional materials especially for the blocks of fabricating nanodevices [2,3]. As important optical materials, rare earth (RE) materials have unique luminescent properties. Taking advantage of size- and shape-dependent properties, RE-doped nanocrystals with desired morphologies will play outstanding roles in building new optoelectronic devices in the near future [4]. A number of synthesis methods, such as hydrotherm [5,6], sol–gel [7], microemulsion [8], combustion [9], and liquid–solid-solution (LSS) [10], have been developed so far to prepare desired nanostructures.

Fluorides have low phonon energies and RE-doped fluoride nanocrystals have been widely studied because of their high quantum efficiencies as luminescent materials and widespread applications in display devices, optical communication, short wavelength solid-state lasers, and so on [11–18]. Especially, YF_3 nanocrystal doped with RE ions is a potential candidate as an efficient phosphor with interesting up/down conversion luminescent properties. For example, Zhang et al. investigated the spectral properties of Eu^{3+}-doped YF_3 nanoparticles [19,20] and Li and Yan studied the upconversion luminescence properties of Yb^{3+}/Er^{3+}-codoped YF_3 nanocrystals [21]. Recently, hexagonal and hollow peanut-like YF_3 nanocrystals were also reported [22,23]. The study on the synthesis and photoluminescence properties of Ln^{3+}-doped YF_3 nanocrystals have become one hot topic in the field of nanosized optical functional materials.

In the present study, YF_3:Eu^{3+} nanobundles, consisting of numerous nanowhiskers with ~500 nm length and ~2 nm diameter, were prepared by a facile microemulsion method. Compared to the YF_3 nanofibers (~3 nm in diameter) synthesized by sonochemistry-assisted hydrothermal route [21], the nanowhiskers are much thinner. The luminescence properties of the nanobundles were investigated in detail and the optimum concentration of Eu^{3+} doped in YF_3 nanobundles was determined.

2. Results and discussion

2.1. Crystal structure and morphology

The crystal structure and phase purity of the sample were analyzed by X-ray diffraction (XRD), as shown in Fig. 1. All the diffraction peaks can be easily indexed to a pure orthorhombic YF_3 (JCPDS 74-0911). No other impurity peaks were detected. The morphology of the product was characterized by observations using scanning electron microscope (SEM) and transmission electron microscope (TEM) as shown in Fig. 2. The magnified

* Corresponding author. Tel.: +86 431 85168240/8325; fax: +86 431 85168240/8325.
E-mail address: wpqin@jlu.edu.cn (W. Qin).

0022-1139/$ – see front matter © 2008 Elsevier B.V. All rights reserved.
doi:10.1016/j.jfluchem.2008.05.003

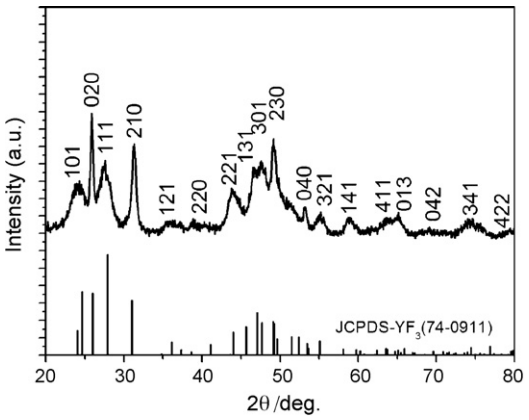

Fig. 1. XRD pattern of YF_3:Eu^{3+} nanobundles.

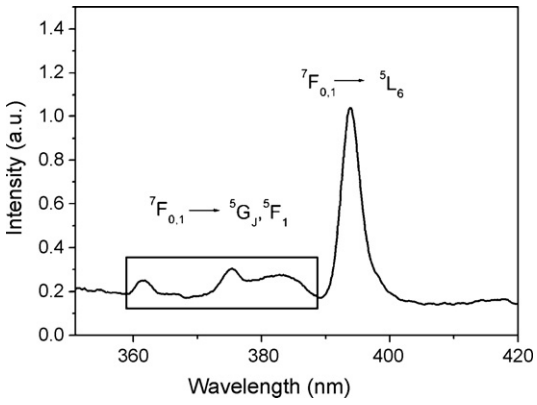

Fig. 3. Excitation spectrum of YF_3:Eu^{3+}(5%) nanobundles monitored at 590 nm.

TEM image of an individual nanobundle indicates that each nanobundle consists of numerous nanowhiskers with a mean length of ~500 nm and a mean diameter of ~2 nm (Fig. 2c). The selected area electron diffraction pattern (inset of Fig. 2c) indicates the polycrystalline structure of YF_3:Eu^{3+} nanobundles. According to the formation mechanism of nanostructures in microemulsion systems reported by Sui et al., nanoparticles formed by constant collision, fusion, and fission of micelles first, and then these nanoparticles self-organized to one-dimension nanostructure [24]. The detailed growth mechanism of nanowhiskers will be discussed in a separate paper.

2.2. Luminescence characteristics

Fig. 3 shows the room-temperature excitation spectrum (monitored at 590 nm) of YF_3:Eu^{3+}(5%) nanobundles. The positions of these excitation peaks are practically identical to the characteristic absorption bands for f–f intra-configuration transitions in trivalent europium [21,25]. The most intense peak is centered at 393 nm with a full width of only ~3.5 nm at half maximum.

No notable excitation peak was observed in the range from 200 nm to 300 nm. This is in accordance with the excitation spectrum of YF_3:Eu^{3+} nanocrystals reported by Li and Yan [21]. In Eu^{3+}-doped systems, charge transfer occurs by electron delocalization from the filled 2p-shell of the ligand to the partially filled 4f-shell of Eu^{3+}. The transition energy is determined by the electronegativity of the ligand [21]. The charge-transfer transition of pure fluoride systems usually exists in the vacuum ultraviolet (VUV) region as a result of high electronegativity. Under current experimental condition, we cannot further explore the VUV-excited fluorescence in the nanobundles.

Fig. 4 shows the room-temperature emission spectrum of YF_3:Eu^{3+}(5%) nanobundles under 393-nm excitation. The $^5D_0 \rightarrow {}^7F_J$ (J = 1, 2, 3, 4) and $^5D_1 \rightarrow {}^7F_J$ (J = 0, 1, 2) transitions were observed. Because the 4f energy levels of Eu^{3+} are hardly affected by the crystal field [19,20], there is no notable shift in the positions of the emission peaks compared to other Eu^{3+}-doped systems [18]. Some of these transitions satisfy magnetic dipole selection rules (ΔJ = 0, ±1 except 0 ↔ 0). The $^5D_0 \rightarrow {}^7F_1$ and $^5D_1 \rightarrow {}^7F_J$ (J = 0, 1, 2) transitions are magnetic-dipole-allowed and their intensities are almost independent on the local environment around Eu^{3+} ions [26]. The $^5D_0 \rightarrow {}^7F_2$ transition is electric-dipole-allowed due to an admixture of opposite parity $4f^{n-1}5d$ states by an odd parity crystal-field component [27,28]. Therefore, its intensity is sensitive to the local structure around Eu^{3+} ions. The $^5D_0 \rightarrow {}^7F_3$ transition exhibits a mixed magnetic dipole and electric dipole character [26]. The $^5D_0 \rightarrow {}^7F_4$ is an electric dipole transition.

It is well known that the intensity ratio of $^5D_0 \rightarrow {}^7F_2$ to $^5D_0 \rightarrow {}^7F_1$ is strongly dependent on the local symmetry of the Eu^{3+} ions. Therefore, Eu^{3+} ions are often used as probes to detect local environments in a matrix. In a site with inversion symmetry the $^5D_0 \rightarrow {}^7F_1$ is dominating, while in a site without inversion symmetry the $^5D_0 \rightarrow {}^7F_2$ is the strongest. In the emission spectrum of YF_3:Eu^{3+}(5%) nanobundles, the $^5D_0 \rightarrow {}^7F_1$ is much stronger than the $^5D_0 \rightarrow {}^7F_2$, indicating the inversion symmetry of Eu^{3+} site [20].

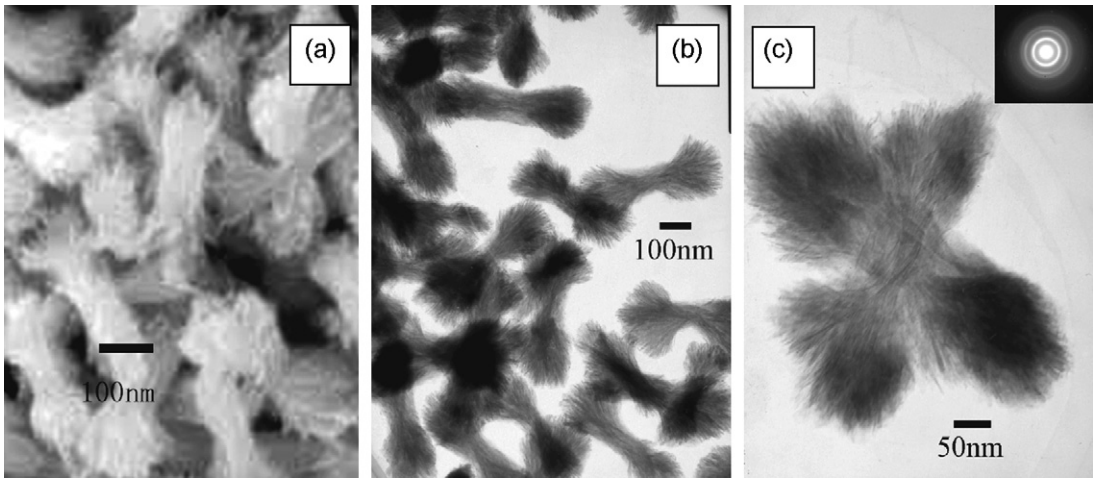

Fig. 2. (a) SEM image of YF_3:Eu^{3+}(5%) nanobundles. (b) TEM image of nanobundles. (c) A crossed nanobundle. Inset: electron diffraction patterns.

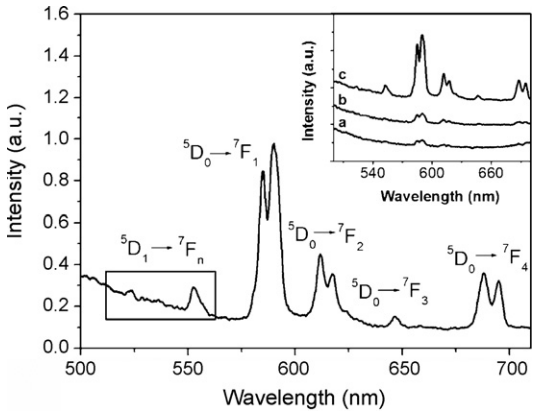

Fig. 4. Emission spectrum of YF_3:Eu^{3+}(5%) nanobundles under 393-nm excitation. Inset: emission spectra of YF_3:Eu^{3+}(5%) nanobundles under different excitation wavelength: (a) 362 nm; (b) 376 nm; (c) 393 nm.

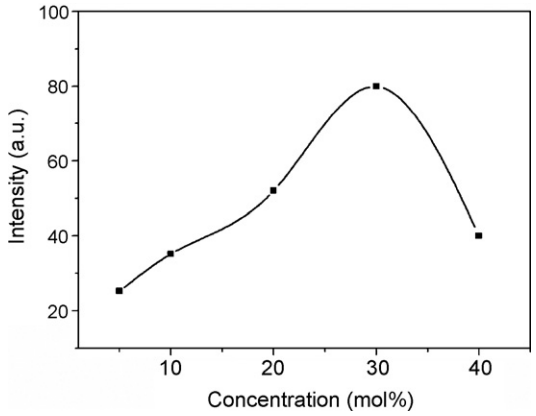

Fig. 5. Dependence of emission intensity of the $^5D_0 \rightarrow {}^7F_1$ transition on Eu^{3+} concentration.

The inset in Fig. 4 presents the emission spectra of YF_3:Eu^{3+}(5%) nanobundles under different excitation wavelength: (a) 362 nm; (b) 376 nm; (c) 393 nm. It can be observed that the emission intensities were the strongest when the excitation was performed at 393 nm.

2.3. Concentration quenching

Fig. 5 shows the relationship between the intensity of 590-nm emission and doping Eu^{3+} concentration. The Eu^{3+} concentration was varied from 0.1 mol% to 40 mol%. The 590-nm emission was hardly observed when the dopant concentration was lower than 5 mol%. Furthermore, the sample with a dopant concentration of 30 mol% shows the highest emission intensity. The peak positions and spectral shapes of emissions were not influenced by Eu^{3+} concentration. The dependence of the intensity ratio of ($^5D_0 \rightarrow {}^7F_2$) to ($^5D_0 \rightarrow {}^7F_1$) on Eu^{3+} concentration indicates that there is no any apparent change in the local symmetry around Eu^{3+} ions with increasing Eu^{3+} concentration. This quenching concentration is much higher than those reported in literatures. Hong and Li reported an optimum Eu^{3+} concentration of about 8 mol% in Gd_2O_3:Eu^{3+} nanocrystals [29] and Sharma reported an optimum Eu^{3+} concentration of 3 mol% for Y_2O_3:Eu^{3+} [30], respectively. However, a similar quenching concentration has been reported by Cui et al [5]. According to Li's explanation, the quenching concentration is mainly determined by the structural characteristic of host [31].

In many cases, the concentration quenching is due to energy transfer from one dopant ion to another until an energy sink in the lattice is reached, which is related to the interaction between dopant ions. For this reason, it is possible to obtain the critical distance (R_c) between donor (activator) and acceptor (quenching site) from the concentration quenching data. Blasse assumed that for the critical concentration the average shortest distance between nearest activator ions is equal to the critical distance [32]. Hence, we can estimate the critical distance by using the following equation:

$$R_c = 2\left(\frac{3V}{4\pi x_c N}\right)^{1/3}$$

where x_c is the critical concentration, N is the number of Y^{3+} ions in a YF_3 unit cell, and V is the volume of YF_3 unit cell (191.17×10^{-30} m^3 in this case). For the critical concentration of 30 mol% Eu^{3+}, according to the above equation, R_c is determined to be about 10.7 Å.

3. Conclusion

In summary, YF_3:Eu^{3+} nanobundles were synthesized in the quaternary reverse microemulsion system with water/CTAB/1-pentanol/cyclohexane and characterized by XRD, SEM, and TEM. The YF_3:Eu^{3+} nanobundles, consisting of numerous nanowhiskers with ~500 nm length and ~2 nm diameter, showed an orthorhombic structure. Under 393-nm excitation, the $^5D_0 \rightarrow {}^7F_1$ transition was much stronger than the $^5D_0 \rightarrow {}^7F_2$ transition, indicating the inversion symmetry of Eu^{3+} site. The emission intensity was the highest for YF_3 nanobundles doped with 30 mol% Eu^{3+}. The dependence of the intensity ratio of ($^5D_0 \rightarrow {}^7F_2$) to ($^5D_0 \rightarrow {}^7F_1$) on Eu^{3+} concentration indicated that there is no apparent change in the local symmetry around Eu^{3+} ions with increasing Eu^{3+} concentration. The critical distance of energy transfer was calculated to be 10.7 Å.

4. Experimental

4.1. Synthesis

Y_2O_3 and Eu_2O_3 (purity >99.99%) were supplied by Shanghai Chemical Reagent Company. Cetyltrimethylammonium bromide (CTAB), cyclohexane, 1-pentanol, NaF, and HCl were supplied by Beijing Chemical Reagent Company, and were of analytical grade. All the reagents and solvents were used as received without further purification. Distilled water was used to prepare solutions. YCl_3 and $EuCl_3$ were prepared by dissolving Y_2O_3 and Eu_2O_3 in 5% HCl, respectively. An aqueous solution consisted of $(1-x)YCl_3$ and $xEuCl_3$ (x = 0.001, 0.01, 0.05, 0.10, 0.20, 0.30, and 0.40) was obtained.

Two identical solutions, denoted as microemulsion I and II, were prepared by dissolving 2.25 g of CTAB in 50 mL of cyclohexane and 2.5 mL of 1-pentanol. The two microemulsions were stirred separately for 30 min, and then 2 mL of 0.5 M $LnCl_3$ (Ln = Y, and Eu) aqueous solution and 2 mL of NaF aqueous solution were added dropwise to microemulsion I and II, respectively. After vigorously stirring, the two optically transparent microemulsion solutions were mixed and stirred for another 1 h. After aging at room-temperature for 72 h, the emulsion mixture was centrifuged at 12000 rpm for 10 min, which caused sedimentation of the product and allowed removal of mother liquor. The product was then washed with distilled water and absolute ethanol in turn, and finally dried in vacuum at 80 °C for 4 h.

4.2. Characterization

Phase identification was performed via X-ray powder diffractometer (XRD, Rigaku RU-200b) using a nickel-filtered Cu Kα

radiation (λ = 1.4518 Å) in the range of $20 \leq 2\theta \leq 80^{\circ}$. The size and morphology were characterized by scanning electron microscope (SEM, KYKY 1000B) and transmission electron microscope (TEM, JEM 2010 with operating voltage of 200 kV). SEM sample was prepared by placing droplets of the ethanol dispersion on silicon wafers and letting the ethanol evaporate in air. TEM sample was prepared by ultrasonic nebulization of ethanolic dispersion on a lacey-film copper grid. The luminescence spectra were measured at room temperature with a Hitachi F-4500 fluorescence spectrophotometer.

Acknowledgements

This research was supported by Natural Science Foundation of China (Grant Nos. 10474096 and 50672030).

References

[1] R.N. Bhargava, D. Gallaghar, X. Hong, A. Nurmikko, Phys. Rev. Lett. 72 (1994) 416.
[2] H. Liu, A.P. Alivisatos, Nano Lett. 4 (2004) 2397.
[3] W. Chen, J.Z. Zhang, A.G. Joly, J. Nanosci. Nanotechnol. 4 (2004) 919.
[4] K. Kawano, K. Arai, H. Yamada, N. Hashimoto, R. Nakata, Sol. Energy Mater. Sol. Cells 48 (1997) 35.
[5] Y. Cui, X. Fan, Z. Hong, M. Wang, J. Nanosci. Nanotechnol. 6 (2006) 830.
[6] X. Wang, Y.D. Li, Chem. Eur. J. 9 (2003) 5627.
[7] A. Patra, C.S. Friend, R. Kapoor, N. Prasad, J. Phys. Chem. B 106 (2002) 1909.
[8] M. Schwuger, K. Stickdom, R. Schomacker, Chem. Rev. 95 (1995) 849.
[9] Y. Tao, G.W. Zhao, W.P. Zhang, S.D. Xia, Mater. Res. Bull. 32 (1997) 501.
[10] L. Wang, Y. Li, Chem. Mater. 19 (2007) 727.
[11] S. Sivakumar, F. Veggel, P. May, J. Am. Chem. Soc. 129 (2007) 620.
[12] Y. Wang, W. Qin, J. Zhang, C. Cao, J. Zhang, Y. Jin, P. Zhu, G. Wei, G. Wang, L. Wang, Chem. Lett. 36 (2007) 1.
[13] X. Wang, J. Zhuang, Q. Peng, Y. Li, Inorg. Chem. 45 (2006) 6661.
[14] G. De, W. Qin, J. Zhang, J. Zhang, Y. Wang, C. Cao, Y. Cui, J. Solid State Chem. 179 (2006) 955.
[15] J. Zhang, W. Qin, J. Zhang, Y. Wang, C. Cao, Y. Jin, G. Wei, G. Wang, L. Wang, J. Nanosci. Nanotechnol. 8 (2007) 1.
[16] C. Li, Z. Quan, P. Yang, J. Yang, H. Lian, J. Lin, J. Mater. Chem. 18 (2008) 1353.
[17] C. Li, J. Yang, Z. Quan, P. Yang, D. Kong, J. Lin, Chem. Mater. 19 (2007) 4933.
[18] C. Li, Z. Quan, J. Yang, P. Yang, J. Lin, Inorg. Chem. 46 (2007) 6329.
[19] M. Zhang, H. Fan, B. Xi, X. Wang, C. Dong, Y. Qian, J. Phys. Chem. C 111 (2007) 6652.
[20] F. Tao, Z. Wang, L. Yao, W. Cai, X. Li, J. Phys. Chem. C 111 (2007) 3241.
[21] R.X. Yan, Y.D. Li, Adv. Funct. Mater. 15 (2005) 763.
[22] J.L. Lemyre, A.M. Ritcey, Chem. Mater. 17 (2005) 3040.
[23] M. Wang, Q. Huang, H. Zhang, X. Chen, Z. Xue, X. You, Cryst. Growth Des. 10 (2007) 2106.
[24] X. Sui, Y. Chu, S. Xing, M. Yu, C. Liu, Colloids Surf. A 251 (2004) 103.
[25] R. Balda, J. Fernández, J.L. Adam, M.A. Arrriandiaga, Phys. Rev. B: Condens. Matter 54 (1996) 12076.
[26] S. Ray, P. Pramanik, J. Appl. Phys. 97 (2005) 094312.
[27] B.R. Judd, Phys. Rev. 127 (1962) 750.
[28] G.S. Ofelt, J. Chem. Phys. 37 (1962) 511.
[29] Y.H. Li, G.Y. Hong, J. Lumin. 45 (1990) 341.
[30] P.K. Sharma, R. Nass, H. Schmidt, Opt. Mater. 10 (1998) 161.
[31] Y. Li, Y. Chang, Y. Lin, Y. Chang, Y. Lin, J. Alloys Compd. 439 (2007) 367.
[32] G. Blasse, Philips Res. Rep. 24 (1969) 131.